Supplementary Information

Electronic Levels of Excess Electrons in Liquid Water

Francesco Ambrosio,* Giacomo Miceli, and Alfredo Pasquarello

Chaire de Simulation à l'Echelle Atomique (CSEA), Ecole Polytechnique Fédérale de Lausanne (EPFL), CH-1015 Lausanne, Switzerland

E-mail: Francesco.Ambrosio@epfl.ch

Phone: +41 21 6933423. Fax: +41 21 693 5419

*To whom correspondence should be addressed

1 Computational details of molecular dynamics simulations

We carry out hybrid-functional molecular dynamics simulations with the PBE0 functional,[1,2] in which the fraction α of Fock exchange is set to 0.40 to achieve a good description of the band gap.[3,4] The van der Waals (vdW) interactions are described through the nonlocal rVV10 scheme[5,6] with the parameter b set to 5.3 to achieve the correct mass density of liquid water.[4]

The empirical tuning of the fraction α of Fock exchange in the PBE0 functional has already been applied to the electronic properties of semiconductors.[7,8] In particular, the accuracy of this computational scheme has been benchmarked by calculating ionization potentials and electron affinities of a large set of materials.[8] Excellent agreement with experiment was achieved for these quantities when the fraction of α was tuned to reproduce the experimental band gap. Employing computational schemes that correctly reproduce the band gap and the band edges of semiconductors and insulators ensures the accurate calculation of redox levels (or charge transition levels of defects in crystalline materials). In fact, an incorrect theoretical description of these quantities is found to dramatically affect the calculated energy levels.[3,7] Furthermore, the self-interaction error in density functional theory is found to deteriorate the description of many systems with unpaired electrons. In order to achieve realistic MD trajectories for some systems, it can be critical to overcome the limitations set by the self-interaction error implied in semilocal density functional descriptions.[9] We here use molecular dynamics simulations at the hybrid functional level to achieve a partial cancellation of the self-interaction error.

All the calculations are performed with the `CP2K` suite of codes.[10] Goedecker-Teter-Hutter pseudopotentials[11] are used to account for core-valence interactions. We use a triple-ζ polarized basis set[12] for the wave functions and a cutoff of 800 Ry for the expansion of the electron density in plane waves. We employ the auxiliary density matrix method with the

cFIT3 auxiliary basis set.[13]

The starting configuration is taken from previous molecular dynamics (MD) simulations of liquid water in the NVT ensemble at the experimental density and performed with the same functional employed in this work.[4] We use periodic supercells of cubic shape containing 64 water molecules, but also employ supercells with 128 water molecules to evaluate finite-size effects. The target temperature is set to 350 K to ensure a frank diffusive motion.[3,4] This choice is conforted by the weak experimental dependence on temperature of both the vertical binding energy[14] and the optical spectrum[15] between 300 and 350 K. For instance, by increasing the temperature from 300 to 350 K, a shift of 0.1 eV is observed in the position of the peak of the measured absorption spectrum.[15] This effect is smaller than the accuracy of the employed methodology ($\sim$0.2 eV). The sampling of the NVT ensemble is ensured by the use of a Nosé-Hoover thermostat.[16,17] For the calculation of the redox level, the convergence of the calculated total-energy differences with respect to the basis set has been checked by placing additional localized basis functions at the center of the hydrated-electron density. The larger basis set leads to a systematic energy correction of 0.07 eV, which is accounted for in the reported results.

We do not explicitly account for nuclear quantum motions. The parameters of the adopted hybrid functional have been set to reproduce the band gap as in the experiment and therefore effectively account for the renormalization due to nuclear quantum effects.[4,18] The redox level of the hydrated electron is expected to be affected by nuclear quantum motions only through a broadening of its distribution, as can be inferred by examining their effect on the localized $1b_1$ state of liquid water.[18] This effect explains why the calculated widths for the distribution of vertical binding energies [Fig. 3 (a) of the main text] and of the $s-p$ absorption spectrum [Fig. 3 (b) of the main text] are smaller than in the experiment. In contrast, we note that reactions involving deprotonation, such as the reduction of the aqueous proton to gaseous hydrogen, are subject to nuclear quantum effects insofar the number of hydrogen nuclei in the simulation cell varies. These effects are accounted for in the determination of

the standard hydrogen electrode reference level (*vide infra*).

2 Grand canonical formulation of solutes in aqueous solution

The free energy of the reduction reaction of liquid water [cf. Eq.(1) of the main text] can be expressed using a grand-canonical formulation of solutes:[3,19]

$$\Delta G(e_{\mathrm{hyd}}) = G[e_{\mathrm{hyd}}] - G[\mathrm{H_2O}(\ell)] - \epsilon_{\mathrm{v}} - \mu, \tag{1}$$

where $G[\mathrm{H_2O}(\ell)]$ is the free energy of liquid water, $G[e_{\mathrm{hyd}}]$ the free energy of the hydrated electron, ϵ_{v} the valence band edge of liquid water, and μ the electron chemical potential. The free-energy difference $G[e_{\mathrm{hyd}}] - G[\mathrm{H_2O}(\ell)]$ can then be expressed as a thermodynamic integral:

$$G[\mathrm{H_2O}(\ell)] - G[e_{\mathrm{hyd}}] = \Delta_{\mathrm{ox}} A_{\mathrm{hyd}} = \int_0^1 \langle \Delta E_{\mathrm{ox}} \rangle_\eta d\eta. \tag{2}$$

$\langle \Delta E_{\mathrm{ox}} \rangle_\eta$ correspond to vertical energy differences averaged over trajectories achieved for different values of the Kirkwood parameter η, which defines the fictitious Hamiltonian introduced in Eq. (3) of the main text. We achieve good convergence with six values of η (0, 0.5, 0.7, 0.8, 0.9, 1). In particular, at $\eta = 0$, $\langle \Delta E_{\mathrm{ox}} \rangle_0$ represents the vertical injection of an electron in liquid water. We calculate this quantity from an MD simulation of 10 ps, after 5 ps of equilibration. At $\eta = 1$, $\langle \Delta E_{\mathrm{ox}} \rangle_1$ is the vertical oxidation energy of e_{hyd}. To calculate this quantity, we start from a structural configuration of liquid water and we add one electron. The electron is found to localize in a cavity within 1 ps. Hence, we perform an equilibration of 5 ps and we calculate electronic properties from a production run of 10 ps. During this time, we do not observe any drifting behaviour of the calculated electronic properties. Similar computational set-ups have been employed for η =0.8 and $\eta = 0.9$. For η =0.5 and 0.7, shorter production runs have been performed (5-7 ps) as no localization of

the partial charge is observed within this time. The redox level μ_{hyd} [cf. Eq. (3) of the main text] is defined as the value of μ for which $\Delta G(e_{\mathrm{hyd}}) = 0$.[3] A similar definition applies for the vertical level μ_{ver} [cf. Eq. (4) of the main text].

To align the calculated energy levels to experimental ones, we make use of the standard hydrogen electrode (SHE). We employ a computational SHE[3,20] based on the reduction of the aqueous hydronium ion:

$$\mathrm{H_3O^+(aq)} + e^- \rightarrow \mathrm{H_2O}(\ell) + \frac{1}{2}\mathrm{H_2(g)}. \tag{3}$$

The respective redox level is given by the following expression:[3]

$$\mu_{\mathrm{SHE}} = \Delta_{\mathrm{dp}} A_{\mathrm{H_3O^+}} - \Delta_{\mathrm{zp}} E_{\mathrm{H_3O^+}} + \epsilon_{\mathrm{v}} + \mu_{\mathrm{H}}. \tag{4}$$

In Eq. (4), $\Delta_{\mathrm{dp}} A_{\mathrm{H_3O^+}}$ is the integral associated to the deprotonation reaction of the hydronium cation, $\Delta_{\mathrm{zp}} E_{\mathrm{H_3O^+}}$ a correction that accounts for the lack of nuclear quantum motions in our MD simulations, and μ_{H} the chemical potential of hydrogen. The SHE level has previously been aligned with respect to the band edges of liquid water for the functional adopted in this work.[4] The connection between the SHE and the vacuum level is established through the experimental relationship, which places the SHE level at 4.45 eV below the vacuum level.[21]

3 Electrostatic finite-size effects

The structural properties of charged solutes in aqueous solution are marginally affected by finite-size effects, as they are found to be already converged for moderate dimensions of the employed supercell (e.g. Fe^{3+} in Ref. 22). At variance, it is well-known that electrostatic finite-size effects affect the calculated energy levels of defects in crystalline materials and redox levels in aqueous solution.[23,24] In the present work, electrostatic finite-size effects in

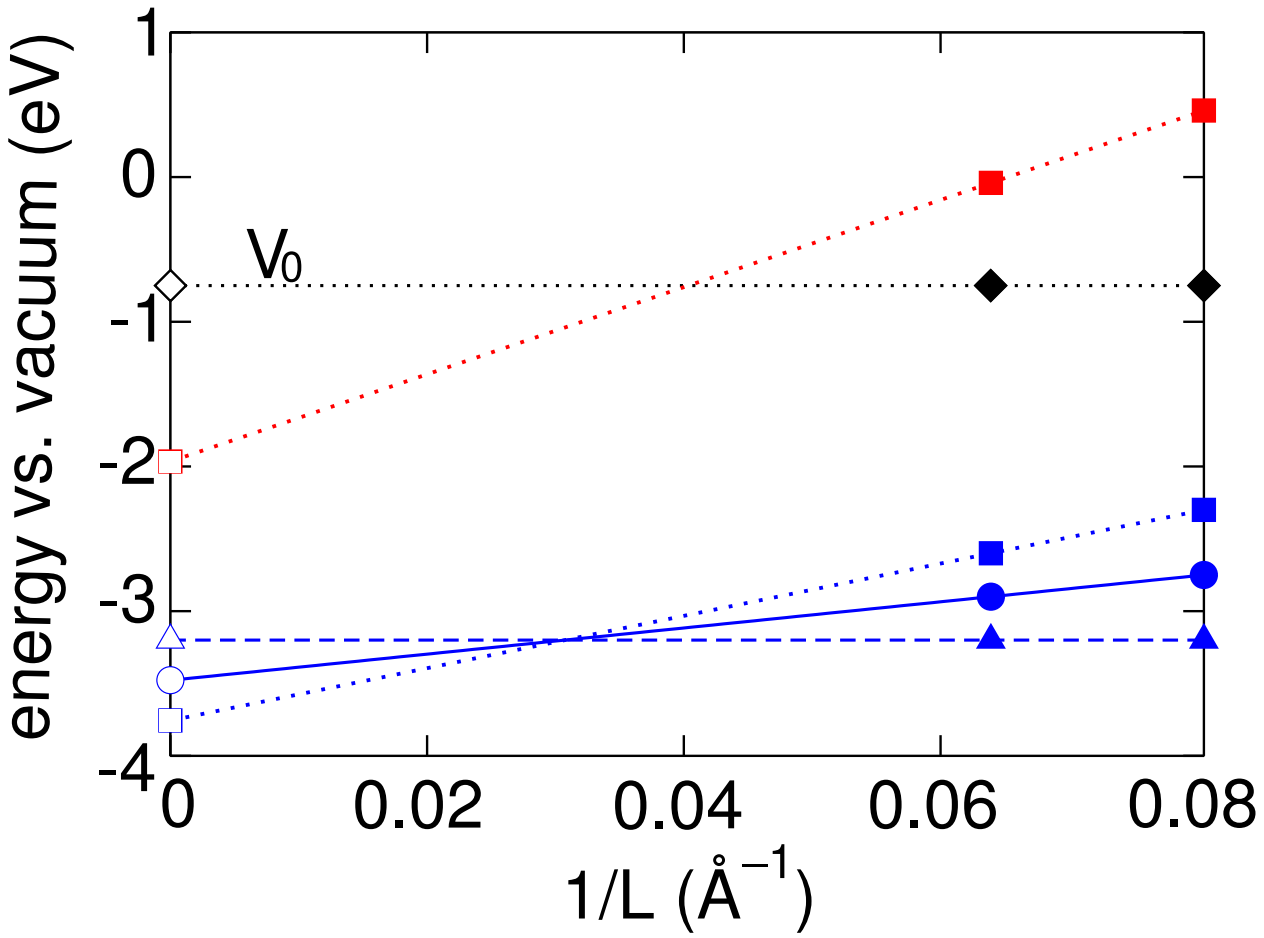

Figure 1: $\mu_{\rm ver}$ (blue circles), $\epsilon_s(1)$ (blue triangles), $\epsilon_s(0)$, (blue squares) and $\epsilon_p(0)$ (red squares) as a function of the inverse size $1/L$ of the supercell. The open symbols refer to the linearly scaled values at $L \to \infty$. The energy scale is referred to the vacuum level via the the standard hydrogen electrode level (cf. main text). The position of V_0 is reported with a dotted black line.

the calculation of $\mu_{\rm ver}$ have been taken into account by linear extrapolation of the values calculated for supercells containing 64 and 128 water molecules to the limit of a supercell of infinite size (cf. Fig. 1). This procedure is consistent with correction schemes available in the literature and implies errors smaller than 0.1 eV for the employed supercells.[23]

The nature of the finite-size effects can be clarified by investigating the Kohn-Sham eigenvalue associated to $e_{\rm hyd}$. In fact, $\mu_{\rm ver}$, which in the main text has been expressed in terms of total-energy differences, can equivalently be calculated using the Kohn-Sham eigenvalues associated to the extra electron. According to Janak theorem, $\mu_{\rm ver}$ given with respect to $\epsilon_{\rm v}$ reads:[25]

$$\begin{aligned}\mu_{\rm ver} &= \langle \Delta E_{\rm ox} \rangle_1 - \epsilon_{\rm v} = \langle E^{-1}[e_{\rm hyd}] - E^0[e_{\rm hyd}] \rangle - \epsilon_{\rm v} \\ &= \int_0^1 \epsilon_s(n) dn - \epsilon_{\rm v}, \end{aligned} \tag{5}$$

where $E^{-1}[e_{\rm hyd}]$ is the total energy of the $e_{\rm hyd}$ system, $E^0[e_{\rm hyd}]$ the total energy of the same structural configuration upon vertical removal of the extra electron, $\epsilon_s(n)$ the eigenvalue associated to the s-like ground state of $e_{\rm hyd}$ as a function of the fractional occupation n. $\epsilon_s(n)$ is integrated between 0 (empty state) and 1 (occupied state). The energy of $\epsilon_s(n)$ is not constant with occupation n, because of the self-interaction effect.[26] Nevertheless, $\mu_{\rm ver}$ can be expressed via the average of the empty and occupied Kohn-Sham eigenvalues:

$$\int_0^1 \epsilon_s(n) dn \simeq \frac{\epsilon_s(1) + \epsilon_s(0)}{2} = \epsilon_s(1/2), \tag{6}$$

leading to:

$$\mu_{\rm ver} = \langle \epsilon_s(1/2) \rangle - \epsilon_{\rm v}. \tag{7}$$

We verify that this approximation is closely satisfied in the present calculations. $\epsilon_s(1)$ is essentially constant with supercell size. In fact, upon the formation of the cavity, the extra electron is screened by the static dielectric constant of liquid water (78.3 at ambient con-

ditions[27]). Therefore, the shift induced by electrostatic finite-size effects on the energy of $\epsilon_s(1)$ is negligible. At variance, the empty state formed upon vertical ionization of $e_{\rm hyd}$ is strongly affected by electrostatic finite-size effects, due to the divergence in the polarization, which is screened only by the electrons of the system (i.e. through the high-frequency dielectric constant of liquid water, 1.68[28]). The self-interaction effect shifts the position of the Kohn-Sham states upon occupation.[26,29] These two effects need to be accounted for in the evaluation of the optical transitions from the s-like ground state to the p-like excited states. In fact, the average total energy difference associated to a generic $s \rightarrow p$ transition reads as follows:

$$\mu_{\rm opt} = \mu_{\rm p} - \mu_{ver}, \tag{8}$$

where μ_p is the vertical ionization energy of $e_{\rm hyd}$ in an excited p-like state, given with respect to $\epsilon_{\rm v}$:

$$\mu_p = \langle E^{-1*}[e_{\rm hyd}] - E^0[e_{\rm hyd}] \rangle - \epsilon_{\rm v}. \tag{9}$$

In Eq. (9), $E^{-1*}[e_{\rm hyd}]$ is the total energy of the $e_{\rm hyd}$ system in an excited p-like state for a structural configuration obtained from a MD simulation of the ground state. In calculating $E^{-1*}[e_{\rm hyd}]$, the s-like ground state is assumed to be unoccupied. Applying Janak theorem[25] to the terms of Eq. (9), we obtain the following expression:

$$\mu_p \simeq \frac{\langle \epsilon_p(1) + \epsilon_p(0) \rangle}{2} \rangle - \epsilon_{\rm v} \simeq \langle \epsilon_p(1/2) \rangle - \epsilon_{\rm v}, \tag{10}$$

where $\epsilon_p(1)$ and $\epsilon_p(0)$ are the eigenvalues associated to the occupied and unoccupied Kohn-Sham states of a p-like state. Therefore, the energy of a $s \rightarrow p$ transition reads as follows:

$$\mu_{\rm opt} = \epsilon_p(1/2) - \epsilon_s(1/2), \tag{11}$$

and can be estimated as:

$$\mu_{\rm opt} = \frac{\epsilon_s(1) + \epsilon_s(0)}{2} - \frac{\epsilon_p(1) + \epsilon_p(0)}{2}. \tag{12}$$

The unoccupied p-like states of $e_{\rm hyd}$ are found to be resonant with the conduction band states, due to electrostatic finite-size and self-interaction effects. However, they can be clearly distinguished from delocalized conduction band states through inspection of the wave-function (i.e. the inverse partecipation ratio and the gyration radius). Therefore, the only term in Eq. (12) which is not directly accessible from our DFT-MD simulations is $\epsilon_p(1)$. In first approximation, assuming that the self-interaction effects on p-like and s-like states are equal, we can reformulate $\mu_{\rm opt}$ in terms of the energy difference between unoccupied states:

$$\mu_{\rm opt} = \epsilon_s(1/2) - \epsilon_p(1/2) \simeq \epsilon_s(0) - \epsilon_p(0). \tag{13}$$

Hence, we use energy differences between unoccupied s- and p-like states to produce the absorption spectrum shown in the main text. However, since p-like states are more diffuse than the ground state (cf. gyration radius in main text), the effect of the self-interaction is likely to be slightly smaller than the one observed for the s-like states. This allows us to estimate a maximum error of 0.2 eV for $\mu_{\rm opt}$.

4 Comparison with previous theoretical results

In this section, we compare the results calculated in this work with those achieved in previous theoretical studies supporting the cavity model. Both the structural properties of the cavity and the energy levels of the hydrated electron are considered.

First, we discuss the structural properties of the cavity. We notice that the majority coordination number calculated in this work (5 in 44 % of the structural configurations) is different from previous single-electron (4 in Refs. 30 and 31), *ab initio* (6 in Ref. 32), and

mixed quantum mechanical-molecular mechanics (QM-MM) calculations (4 in Ref. 33). The inclusion of van der Waals interactions has already been found to provide higher coordination numbers in molecular dynamics simulations of pure liquid water. In fact, the fifth water molecule (the so-called interstitial water molecule) gets closer to the first coordination shell as dispersion interactions tend to stabilize compact structural motifs.[4] An analogous effect accounts for the majority fivefold coordination number in the case of the hydrated electron. It should be noted that fourfold coordination and sixfold coordination are also encountered in 34.2% and 15% of the structural configurations, respectively, thus indicating noticeable fluctuations of the coordination shell. Our average coordination number is smaller than the one found in Ref. 32. However, the cavity proposed by Boero *et al.* is more elongated than that found in this work. This is evident from the different positions of the peaks in the WFC-O radial distribution functions.

As far as the gyration radius is concerned, we notice that results achieved with different methods agree within 0.4 Å, therefore indicating a similar localization of the excess electron. However, the inspection of the radial distribution functions allows us to observe noticeable differences in the localization of the extra electron. The radial distribution functions in Refs. 32, 30, and 31 indicate that the electron density is almost completely residing in the cavity. In fact, the gyration radius of the wave-function is found to be systematically smaller than the size of the first coordination shell, the latter being defined by the average distance between the center of the electron density and the surrounding O atoms. At variance, in the present work, the size of the first coordination shell corresponds to the gyration radius of the wave function, similarly to Ref. 33. Therefore, our result supports a physical picture in which the electron density extends up to the first oxygen coordination shell.

Hence, we compare the calculated energy levels. Our study provides an average value of $\mu_{\mathrm{ver}} = -3.47$ eV with respect to the vacuum level, well inside the experimental range, in contrast with previous studies that overestimated[30,34] or underestimated[33] this quantity. In regard to μ_{opt}, excellent agreement with experiment has been found in various studies.

Table 1: Majority coordination number n_c, gyration radius r_g (Å), and position of the peaks in the radial distribution functions, d_H and d_O for H and O respectively (Å), from this work and from previous computational studies.

	n_c	r_g	d_H	d_O
This work	5	2.49	1.5	2.5
Uhlig *et al.*[33]	4	2.44	1.5	2.4
Boero *et al.*[32]	6	2.20	1.5	2.9
Jacobson and Herbert[30]	4	2.25	1.7	2.9
Turi *et al.*[31,34]	4	2.12	2.1	3.0

However, this could be fortuitous and due to error cancellations. For example, in Ref. 32 the p-like states are found to be apparently resonant with the conduction band states, an effect that is caused by electrostatic finite-size effects and the self-interaction error. Therefore, the position of the calculated peak is influenced by the position of the conduction band edge, the latter being not correctly reproduced by the employed functional. In Ref. 35, the authors calculate the optical spectrum with a long-range separated density functional,[36] where the long-range parameter is tuned. The results appear to be largely affected by this choice as two different tuning procedures were found to provide μ_{opt} differing by as much as $\sim$0.8 eV. A third result found using the BLYP[37,38] functional is yet different (1.3 eV). However, it remains unclear to what extent the positions of the delocalized band states are affected by the use of different functionals. Finally, we observe the value of μ_{hyd} calculated in this work is the first *ab initio* determination of this level in an all-DFT-based model of the condensed phase, as previous estimates have been obtained from cluster studies. Hence, we remark that the comprehensive agreement achieved for the three energy levels of the hydrated electron should be regarded as strong support for the validity of the employed computational approach.

References

(1) Perdew, J. P.; Ernzerhof, M.; Burke, K. Rationale for Mixing Exact Exchange with Density Functional Approximations. *J. Chem. Phys.* **1996**, *105*, 9982–9985.

(2) Adamo, C.; Barone, V. Toward Reliable Density Functional Methods without Ad-

Table 2: Values of μ_{ver}, μ_{opt}, and μ_{hyd} from this work, from previous computational studies, and from the experiment. μ_{ver} and μ_{hyd} are given with respect to the vacuum level.

	μ_{ver}	μ_{opt}	μ_{hyd}
This work	−3.47	1.75	−1.28
Uhlig *et al.*[33,35]	−3.00	1.3-2.4	
Boero *et al.*[32]		1.7	
Jacobson and Herbert[30]	−3.7	1.7	
Turi *et al.*[31,34]	−3.9	1.92	
Expt.[14,15,39,40]	−3.3-3.6	1.7	−1.47

justable Parameters: The PBE0 Model. *J. Chem. Phys.* **1999**, *110*, 6158–6170.

(3) Ambrosio, F.; Miceli, G.; Pasquarello, A. Redox Levels in Aqueous Solution: Effect of van der Waals Interactions and Hybrid Functionals. *J. Chem. Phys.* **2015**, *143*, 244508.

(4) Ambrosio, F.; Miceli, G.; Pasquarello, A. Structrural, Dynamical and Electronic Properties of Liquid Water: a Hybrid Functional Study. *J. Chem. Phys. B* **2016**, *120*, 7456–7470.

(5) Vydrov, O. A.; Van Voorhis, T. Nonlocal van der Waals Density Functional: The Simpler the Better. *J. Chem. Phys.* **2010**, *133*, 244103.

(6) Sabatini, R.; Gorni, T.; de Gironcoli, S. Nonlocal van der Waals Density Functional Made Simple and Efficient. *Phys. Rev. B* **2013**, *87*, 041108.

(7) Alkauskas, A.; Broqvist, P.; Pasquarello, A. Defect Levels through Hybrid Density Functionals: Insights and Applications. *Phys. Status Solidi B* **2011**, *248*, 775–789.

(8) Chen, W.; Pasquarello, A. Band-edge Positions in GW: Effects of Starting Point and Self-consistency. *Phys. Rev. B* **2014**, *90*, 165133.

(9) Marsalek, O.; Elles, C. G.; Pieniazek, P. A.; Pluharova, E.; VandeVondele, J.; Bradforth, S. E.; Jungwirth, P. Chasing Charge Localization and Chemical Reactivity Following Photoionization in Liquid Water. *J. Chem. Phys.* **2011**, *135*, 224510.

(10) VandeVondele, J.; Krack, M.; Mohamed, F.; Parrinello, M.; Chassaing, T.; Hutter, J. Quickstep: Fast and Accurate Density Functional Calculations using a Mixed Gaussian and Plane Waves Approach. *Comput. Phys. Commun.* **2005**, *167*, 103 – 128.

(11) Goedecker, S.; Teter, M.; Hutter, J. Separable Dual-space Gaussian Pseudopotentials. *Phys. Rev. B* **1996**, *54*, 1703–1710.

(12) Dunning, T. H. Gaussian Basis Sets for Use in Correlated Molecular Calculations. I. The Atoms Boron through Neon and Hydrogen. *J. Chem. Phys.* **1989**, *90*, 1007–1023.

(13) Guidon, M.; Hutter, J.; VandeVondele, J. Auxiliary Density Matrix Methods for Hartree−Fock Exchange Calculations. *J. Chem. Theory Comput.* **2010**, *6*, 2348–2364.

(14) Tang, Y.; Shen, H.; Sekiguchi, K.; Kurahashi, N.; Mizuno, T.; Suzuki, Y.-I.; Suzuki, T. Direct Measurement of Vertical Binding Energy of a Hydrated Electron. *Phys. Chem. Chem. Phys.* **2010**, *12*, 3653–3655.

(15) Jou, F.-Y.; Freeman, G. R. Temperature and Isotope Effects on the Shape of the Optical Absorption Spectrum of Solvated Electrons in Water. *J. Phys. Chem.* **1979**, *83*, 2383–2387.

(16) Nosé, S. A Unified Formulation of the Constant Temperature Molecular Dynamics Methods. *J. Chem. Phys.* **1984**, *81*, 511–519.

(17) Hoover, W. G. Canonical Dynamics: Equilibrium Phase-space Distributions. *Phys. Rev. A* **1985**, *31*, 1695–1697.

(18) Chen, W.; Ambrosio, F.; Miceli, G.; Pasquarello, A. *Ab initio* Electronic Structure of Liquid Water. *Phys. Rev. Lett.* **2016**, *117*, 186401.

(19) Todorova, M.; Neugebauer, J. Extending the Concept of Defect Chemistry from Semiconductor Physics to Electrochemistry. *Phys. Rev. Appl.* **2014**, *1*, 014001.

(20) Cheng, J.; Sprik, M. Alignment of Electronic Energy Levels at Electrochemical Interfaces. *Phys. Chem. Chem. Phys.* **2012**, *14*, 11245–11267.

(21) Trasatti, S. The Absolute Electrode Potential: an Explanatory Note (Recommendations 1986). *Pure Appl. Chem.* **1986**, *58*, 955–966.

(22) Bogatko, S. A.; Bylaska, E. J.; Weare, J. H. First Principles Simulation of the Bonding, Vibrational, and Electronic Properties of the Hydration Shells of the High-Spin Fe^{3+} Ion in Aqueous Solutions. *J. Phys. Chem. A* **2010**, *114*, 2189–2200.

(23) Komsa, H.-P.; Rantala, T. T.; Pasquarello, A. Finite-size Supercell Correction Schemes for Charged Defect Calculations. *Phys. Rev. B* **2012**, *86*, 045112.

(24) Freysoldt, C.; Grabowski, B.; Hickel, T.; Neugebauer, J.; Kresse, G.; Janotti, A.; Van de Walle, C. G. First-principles Calculations for Point Defects in Solids. *Rev. Mod. Phys.* **2014**, *86*, 253–305.

(25) Janak, J. F. Proof that $\frac{\partial E}{\partial n_i} = \epsilon$ in Density-functional Theory. *Phys. Rev. B* **1978**, *18*, 7165–7168.

(26) Dreizler, R. M.; Gross, E. K. *Density Functional Theory: an Approach to the Quantum Many-body Problem*; Springer Science & Business Media, 2012.

(27) Lide, D.; Haynes, W. *CRC Handbook of Chemistry and Physics: a Ready-reference Book of Chemical and Physical Data*; Boca Raton, Fla: CRC, 2009.

(28) Nabokov, O. A.; Lyubimov, Y. A. High-frequency Dielectric Constant of Water and Determination of the Kirkwood Correlation Factor. *J. Struct. Chem.* **1987**, *27*, 731–736.

(29) Slater, J. C. Statistical Exchange-correlation in the Self-consistent Field. *Adv. Quantum Chem.* **1972**, *6*, 1–92.

(30) Jacobson, L. D.; Herbert, J. M. A One-electron Model for the Aqueous Electron that Includes Many-body Electron-water Polarization: Bulk Equilibrium Structure, Vertical Electron Binding Energy, and Optical Absorption Spectrum. *J. Chem. Phys.* **2010**, *133*, 154506.

(31) Turi, L.; Borgis, D. Analytical Investigations of an ElectronâĂŞwater Molecule Pseudopotential. II. Development of a New Pair Potential and Molecular Dynamics Simulations. *J. Chem. Phys.* **2002**, *117*, 6186–6195.

(32) Boero, M.; Parrinello, M.; Terakura, K.; Ikeshoji, T.; Liew, C. C. First-principles Molecular-Dynamics Simulations of a Hydrated Electron in Normal and Supercritical Water. *Phys. Rev. Lett.* **2003**, *90*, 226403.

(33) Uhlig, F.; Marsalek, O.; Jungwirth, P. Unraveling the Complex Nature of the Hydrated Electron. *J. Phys. Chem. Lett.* **2012**, *3*, 3071–3075.

(34) Madarász, Á.; Rossky, P. J.; Turi, L. Interior- and Surface-bound Excess Electron States in Large Water Cluster Anions. *J. Chem. Phys.* **2009**, *130*, 124319.

(35) Uhlig, F.; Herbert, J. M.; Coons, M. P.; Jungwirth, P. Optical Spectroscopy of the Bulk and Interfacial Hydrated Electron from Ab Initio Calculations. *J. Phys. Chem. A* **2014**, *118*, 7507–7515.

(36) Iikura, H.; Tsuneda, T.; Yanai, T.; Hirao, K. A Long-range Correction Scheme for Generalized-gradient-approximation eEchange Functionals. *J. Chem. Phys.* **2001**, *115*, 3540–3544.

(37) Becke, A. D. Density-functional Exchange-energy Approximation with Correct Asymptotic Behavior. *Phys. Rev. A* **1988**, *38*, 3098.

(38) Lee, C.; Yang, W.; Parr, R. G. Development of the Colle-Salvetti Correlation-energy Formula into a Functional of the Electron Density. *Phys. Rev. B* **1988**, *37*, 785.

(39) Shreve, A. T.; Yen, T. A.; Neumark, D. M. Photoelectron Spectroscopy of Hydrated Electrons. *Chem. Phys. Lett.* **2010**, *493*, 216–219.

(40) Schwarz, H. A. Enthalpy and Entropy of Formation of the Hydrated Electron. *J. Phys. Chem.* **1991**, *95*, 6697–6701.